ENVIRONMENTAL RESEARCH
WATER

LETTER

Potable water sources in a contaminated temperate peatland resistant to acute impacts but vulnerable to legacy effects of extreme wildfire

Abbey L Marcotte[1,*], Juul Limpens[1,*], Claire M Belcher[2], Richard C Chiverrell[3], Gareth D Clay[4], Stefan H Doerr[5], Stefan Krause[6], Kieran Khamis[6], Rúna Í Magnússon[1], Jonay Neris[5,7], João Pedro Nunes[8], David P Pompeani[9], Cristina Santín[5,10], Emma L Shuttleworth[4], Sami Ullah[6], Jeff Warburton[11] and Nicholas Kettridge[6,*]

[1] Plant Ecology and Nature Conservation group, Wageningen University, Wageningen 6708 PB, The Netherlands
[2] wildFIRE Lab, University of Exeter, Exeter EX4 4QJ, United Kingdom
[3] Department of Geography, University of Liverpool, Liverpool L69 7ZT, United Kingdom
[4] Department of Geography, University of Manchester, Manchester M13 9PL, United Kingdom
[5] Centre for Wildfire Research, Swansea University, Swansea SA2 8PP, United Kingdom
[6] School of Geography, Earth and Environmental Sciences, University of Birmingham, Birmingham B15 2TT, United Kingdom
[7] Universidad de La Laguna, Tenerife 38206, Spain
[8] Soil Physics and Landscape Management group, Wageningen University, Wageningen 6708 PB, The Netherlands
[9] Department of Natural Resources and Environmental Management, University of Hawai'i at Mānoa, Honolulu, HI 96822, United States of America
[10] Biodiversity Research Institute (IMIB), CSIC-University of Oviedo-Principality of Asturias, Oviedo 33006, Spain
[11] Department of Geography, Durham University, Durham DH1 3LE, United Kingdom
[*] Authors to whom any correspondence should be addressed.

E-mail: abbeymarcotte@gmail.com, juul.limpens@wur.nl and n.kettridge@bham.ac.uk

Keywords: water security, legacy metal pollutants, wildfire impacts, climate change

Supplementary material for this article is available online

OPEN ACCESS

RECEIVED
16 December 2024

REVISED
16 April 2025

ACCEPTED FOR PUBLICATION
24 April 2025

PUBLISHED
2 May 2025

Abstract

Climate change is increasing wildfire frequency and severity, expanding into ecosystems less historically prone to wildfires, such as temperate peatlands. These peatlands are significant potable water sources that have accumulated legacy contaminants for decades. A major concern and uncertainty for ecosystem health and drinking water supply is the timing and magnitude of pollutant release, particularly potentially harmful metals, following extreme disturbances. Here, we examine mobilisation of legacy metals in a contaminated temperate blanket peatland following extreme drought and wildfire occurrence, focussing on key metal sources, transport pathways and deposition on the lake-bed of the receiving reservoir. We found that erosion of metal-rich hillslope peat and ash peaked three months post-wildfire, particularly in extreme burn severity areas, contributing to substantial deposition of metal-rich material in the receiving reservoir. Elevated metal concentrations in suspended sediments were observed nine months post-wildfire during spring rainstorm events. Dissolved metals in the streamflow were comparatively orders of magnitude lower, but displayed similar timing in concentration increases. Together this indicates limited acute but potential chronic impacts that extend beyond our study's monitoring period. These pathways can present different challenges for managing water supplies. Our findings provide critical insights into the spatio-temporal dynamics of metal transport in peatlands following severe drought and wildfire. Understanding these pathways is essential for assessing current and future risks to water quality and developing targeted management strategies in northern peatland regions that are reliant on peat-rich catchments for drinking water and that are increasingly vulnerable to climate-induced disturbances.

1. Introduction

Storing ~10% of globally available freshwater (Joosten and Clarke 2002), peatlands are a core freshwater and potable water resource that form a key component of regional water security solutions, notably at high latitudes (Xu *et al* 2018a, 2018b). Intact healthy peatlands regulate water quality by accumulating contaminants in their organic profiles and buffering downstream water sources by intercepting precipitation (Brown *et al* 2000). More recently, peatlands in proximity to post-industrial areas, such as those in the UK, have accumulated atmospherically derived contaminants (Renberg *et al* 1994, Garcés-Pastor *et al* 2023)—a process that began at least ca. 900 BCE (McCarter *et al* 2024). The accumulation of potentially toxic metals, including lead in surface peat deposits, provides a source of legacy contamination that poses risks to drinking water supplies (McCarter *et al* 2024). The capability of peatlands to store contaminants may become compromised when they are disturbed or become degraded (Price *et al* 2023). Disturbances can result from climate-related (e.g. drought, wildfires) or anthropogenic disturbances (e.g. controlled or accidental burning, grazing or drainage), and thus may shift peatland ecosystems from contaminant sinks into sources (Price *et al* 2023, Sutton *et al* 2024).

The increased intensity and severity of climate-change induced drought is already straining the global potable water resource, with more severe impacts expected in the future (Paul *et al* 2022). In addition to more frequent droughts, the frequency, area and severity of wildfires are also projected to increase, even in peatland-dominated regions historically less prone to wildfire (Bowman *et al* 2020, Jones *et al* 2022). It is of concern that increases in wildfire activity may unlock contaminants formerly retained within the peat, potentially resulting in, or at least accelerating, contaminant delivery to surface waters, including drinking water reservoirs. Burning from wildfires can cause release of these contaminants via the combustion of organic material (Agbeshie *et al* 2022), which can lead to changes in soil chemistry (Wu *et al* 2022). Production of ash changes soils texture and soil water infiltration (Bodí *et al* 2014). Ash and other burnt material may be transported to drinking water reservoirs through dissolution and solute transport, or erosion and transfer of particulate matter (Liu *et al* 2023).

While water quality responses in traditionally fire-prone regions without peatlands provide a framework of potential impacts and mitigation actions (Nunes *et al* 2018), the ability to transfer that knowledge is unclear as there are limited studies on how wildfires impact temperate peatland areas (McCarter *et al* 2023). Water quality risks in peatlands are likely to be different due to their distinct hydrological functioning and storage abilities, biogeochemical processes and subsequently their specific wildfire dynamics. Severe peatland wildfires can smoulder through peat deposits (Benscoter *et al* 2011, Marcotte *et al* 2022), directly interacting with legacy contaminant stores and producing deep ash layers potentially rich in potentially toxic metals that are available for transport into waterways (Sánchez-García *et al* 2023). Severe wildfires typically occur under drought conditions, thus often coupling the negative impacts of both disturbances, potentially resulting in compound impacts on peatland biogeochemical and (eco)hydrological processes (McCarter *et al* 2024). Post-fire changes in hydrological fluxes, notably evapotranspiration and water storage capacity (Kettridge *et al* 2015), will modify the catchment water balance. Near-surface hydrological processes may be altered through ash that can seal soil macropores (Bodí *et al* 2014) and through the development of drought- and fire-induced hydrophobic peat surfaces, thus reducing infiltration and enhancing surface erosion that can cause flashier hydrological responses to precipitation (Holden 2006, Brown *et al* 2015, Shuttleworth *et al* 2019). These interacting factors may induce acute impacts on water quality during drought periods when regional water security is already under stress (Robinne *et al* 2021). Finally, increases in frequency and intensity of heavy precipitation events (IPCC 2022) may exacerbate post-wildfire erosion and transport of sediments and burnt materials laden with potentially harmful metals.

Here we capitalise on a rare high-severity catchment-scale wildfire in a contaminated temperate peatland (2018 Stalybridge wildfire, Peak District, UK). This study addresses a critical research gap (McCarter *et al* 2023, 2024) in our understanding of the fate and transport of potentially harmful metals from a blanket peat system in the aftermath of a severe wildfire and drought period. Specifically, we aim to determine how the compound impact of wildfire and drought induce acute water quality impacts by quantifying (1) the intensification of potentially toxic metal contamination in ash and hillslope (surface peat) deposits within areas of different burn severities; (2) the mobilisation and erosion of deposits under intense summer and spring rainfall events; and (3) the transport and deposition within rivers and receiving reservoirs. We measured metals in ash and peaty soil deposits on the hillslopes. The mobility of ash and burnt materials was assessed using sediment trapping fences, where metal concentrations in captured sediments were also quantified. We captured a broad range of solute and metal-laden suspended sediments in streamflow during five rainstorm events over nine months post-wildfire. These included the first two storm events post-wildfire (Storm 1 and 2), one autumn storm (Storm 3) and two spring storms (Storm 4 and 5) including the highest discharge event of the monitoring period. Finally, we analysed the amount of metals in reservoir surface

sediments. Understanding post-wildfire temporal patterns and drivers of contaminant mobilisation in temperate peatlands is crucial, especially when two key climate-induced disturbances—extreme drought and wildfire—act in concert. This knowledge is essential for adequate risk assessment and the development mitigation measures (McCarter *et al* 2023, 2024).

2. Materials and methods

2.1. Study area description

Fieldwork was conducted within an upland blanket peatland east of Manchester, England, burnt by the Stalybridge Moor wildfire (often referred to as the Saddleworth Moor wildfire; coordinates: 53.511266° N, 1.996026° W) in summer 2018. This wildfire lasted from 24 June to 18 July 2018 and affected a total area of ∼18 km^2 (figure 1(A)). Also, it was one of the largest wildfires in the UK in recent years (Graham *et al* 2020, Forestry Commission 2023), having burnt ∼18 km^2 across Stalybridge Moor. The region has been heavily impacted by industrial pollution since the beginning of the 19th century due to its downwind proximity to industrial towns notably Manchester, Sheffield and Oldham, and peatlands have received substantial inputs of metals that have been stored as legacy pollutants in the peat profile as a result (Rothwell *et al* 2007). The catchment is underlain by Carboniferous Lower Kinderscout Grit—Sandstone, formed between 322 and 321.5 million years ago (BGS Geology Viewer 2024), and additional deposits consist of re-worked weathered soils and colluvium from early glaciations. The catchment consists of strongly sloping areas near the main stream channel where water quality measurements were conducted (figures 1(A) and (B)) and flatter peat plateaus in the headwaters. The network of gullies dissects the landscape and erodes down to bedrock in many areas. Vegetation consists mainly of heather (*Calluna vulgaris*), cotton grass (*Eriophorum vaginatum*), crowberry (*Empetrum nigrum*), bilberry (*Vaccinium myrtillus*) bracken (*Pteridium aquilinum*) and heath star moss (*Campylopus introflexus*). *Sphagnum* spp. occurs sparsely in wetter areas near gullies and the stream and some Silver birch (*Betula pendula*) are present in riparian areas of the stream. A detailed study area description can be found in Marcotte *et al* (2024).

2.2. Determining burn severity

The burn severity analysis was created with difference Normalised Burn Ratio map (hereafter dNBR) (Keeley 2009, Chafer *et al* 2016) using Landsat images 24 June 2018 (pre-fire) to 14 July 2018 (post-fire). Burn severity classes were also established in the field. The *in situ* burn severity assessment was scored after an adaptation of the indices found in Ryan and Noste (1985), where classes ranged from 1–5. While patchy burning did occur, many areas burnt at the highest burn severity (class 5), whereas lower severity classes (1 & 2) occurred less frequently.

2.3. Ash and peaty soil sampling procedures, chemical composition and leaching properties

Sampling of peaty soil and ash were conducted at a few locations where burn severity was determined *in situ*. Ash loads were determined before any rainfall occurred (9–10 July) by quantitatively sampling ash along three transects at each of the two main burn severities: high severity (HS) and extreme severity (ES) (30 points of 20 cm × 20 cm per severity), following standard procedures. After the first rainfall event (Storm 1; figures 1(D) and (E)), eight ash and peaty soil composite samples were taken in the selected burn severities ($n = 4$ per burn severity in 20 cm × 20 cm plots) to be analysed for chemical composition (i.e. concentration of elements) following the same protocol as ash samples. Laboratory analysis of total concentration of elements in peat and ash samples, as well as their readily water-dissolvable concentrations. Using the concentration of metals in the sampled ash and the underlying burnt peaty soils, we calculated an enrichment ratio (ER) (ash-to-underlying soil) to assess the extent to which metals were concentrated in the ash layer following the wildfire, which has implications for metal mobility and distribution in the landscape.

We determined the total concentration of elements for each ash and peaty soil sample collected *in situ* after methods described in Sánchez-García *et al* (2023). Briefly, chemical parameters, including pH and EC (electric conductivity), the total concentration of elements (acid digest) of major nutrients (C, Ca, Mg, N, Na, P) and trace metals (Al, As, Cd, Cr, Cu, Fe, Hg, Mn, Ni, Pb and Zn), and the readily dissolvable concentration (in water extracts) of Al, Ca, F, Fe, Mg, Mn, Na, NH_4^+, $NO3^-$ and DOC (dissolved organic carbon) and P. The pH and EC of samples were determined in water, using an ash-to-water mass ratio of 1:20 after stirring for 5 min and waiting for 10 min (Buurman 1996). The total concentrations of the above listed elements were extracted from the ash samples (0.25 g) by microwave-assisted acid digestion (9 ml of 14.4 M HNNO3, 3 ml of 12 M HCl, 200 °C for 45 min) according to EPA Method 3051 A and determined by ICP-OES spectrometry (Perkin Elmer, Optima 4300DV). Total N and C concentrations were determined using a Total Analyzer Leco TruSpec CHN (Leco Corp., St Joseph, MI, USA).

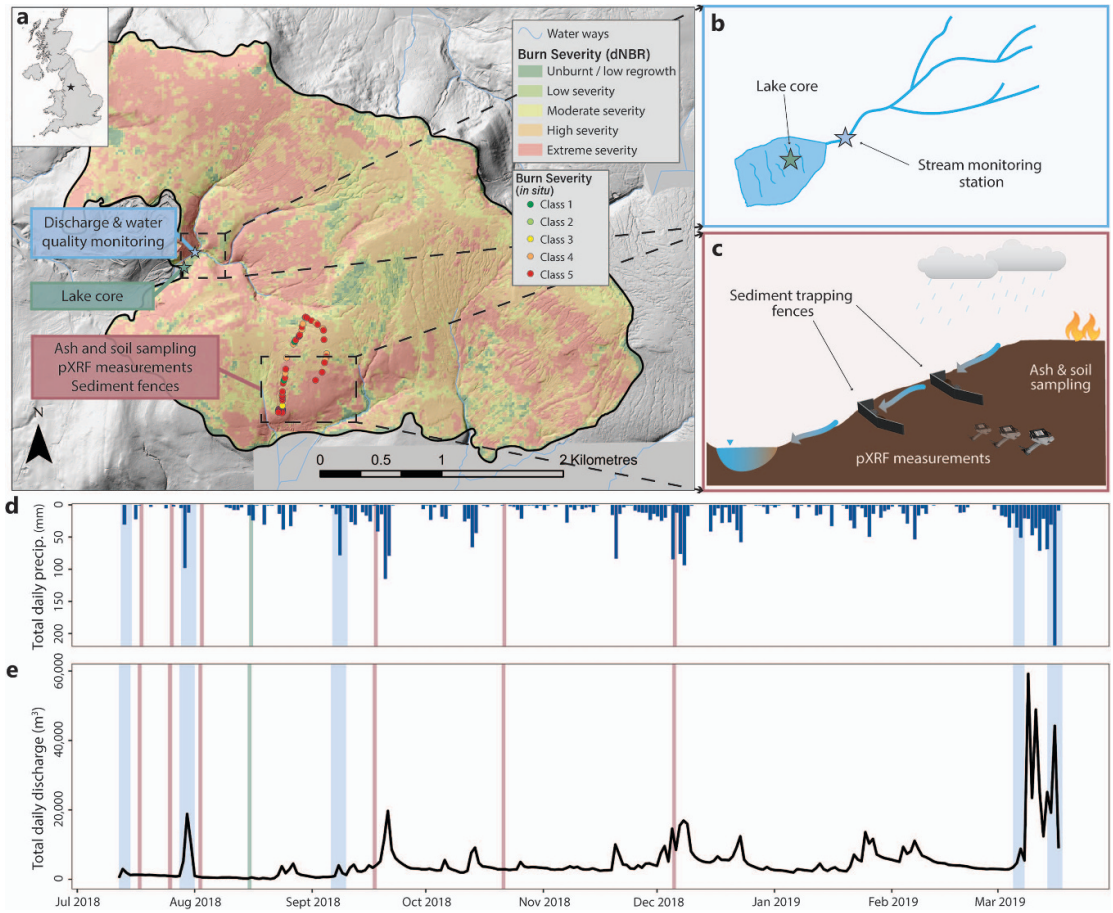

Figure 1. Study area and monitoring design | (a) Study area and location within England. Burn severity variations of the entire study area is shown with normalised burn ratio classifications (dNBR). Burn severity classes (1–5) were also characterised *in situ* shown by the red, orange, yellow and green dots. Sampling areas are indicated with a black dotted-line box and a coloured star; (b) schematic illustration (planar view) the stream monitoring and lake core sampling locations; (c) schematic illustration (cut-view) of hillslope sampling procedures; (d) daily summary of precipitation and (e) daily summary of discharge measured at the stream monitoring station. The blue lines represent the timing of the five rainstorm events highlighted in this study. The red lines indicate the timing of metals measured at the hillslope sampling location, both with ash and peaty soil sampling and pXRF surveys. The green line represents when the lake core was obtained.

Readily dissolvable concentrations of elements from peaty soils and wildfire ash samples were determined using leaching tests described in Hageman (2007) to determine the amount of elements that may be mobilised by water. A full description of the chemical characterisation methods and quality checks are in the supplementary material.

2.4. Field-portable x-ray fluorescence (pXRF) surveys

Field pXRF readings were taken to map and spatially characterise surface metal concentrations along the hillslope (supplementary figure 1). The surface consisted of ash, charcoal and peaty soils. A 125 m transect was sampled at ~5 m intervals, totalling 25 *in situ* readings. Measurements were also obtained in a gridded pattern on the burnt hillslope to better characterise potential small-scale variability of metal concentrations. The grid sampling consisted of five transects spaced ~5 m apart. Each sampling transect consisted of 16 pXRF readings spaced ~2 m apart, totalling 80 pXRF measurements at the grid sampling area. Data was collected using a handheld Niton XL3t 900 XRF analyser, where we used the 'soil' function calibration and analysis time was 120s following methodology and recommendations outlined in Shuttleworth *et al* (2014).

Eighteen confirmatory samples from the field were randomly collected at select pXRF reading sites for calibration and data quality assessment. Elemental concentrations for the 18 samples were determined using ICP-OES (Perkin Elmer Optima 2100 DV) at the Department of Geography at University of Manchester, UK based on BS EN 22036:2008 for the determination of trace elements in Soils by ICP-OES. Sample preparation was done by Microwave Digestion in a CEM Mars Xpress accelerated reaction system using Aqua Regia the digestion reagent. This method uses a 7 point linear calibration with a 99.999% minimum regression, with an internal standard to correct for instrument drift and matrix interferences. Results are quantified against this curve in mg l^{-1}, or ppm, at a limit of detection (LOD) of 0.005 mg l^{-1}. Each sample was measured three

times, and an average of these replicates is calculated by the instrument. The %RSD variance between each replicate is less than 2.5%.

Elemental field values can then be converted to the lab equivalent values. Parameters produced by linear regression analysis were used to assess the strength, precision and accuracy of the relationship between *in situ* pXRF measurements and ICP derived data. Cu, Ni and Pb pXRF measurements were converted based on the slope of the relationship between the pXRF and ex situ ICP-OES derived data ($n = 18$). The slope for each sample is as follows: Cu = 0.530 ($R^2 = 0.787$); Ni = 0.503 ($R^2 = 0.6596$); Pb = 0.518 ($R^2 = 0.8174$). No pXRF data for Al was obtained.

2.5. Erosion monitoring at hillslope scale

Twelve erosion plots with sediment fences were installed after the wildfire was controlled (19 July 2018)—six on a high burn severity area and six on an extreme burn severity area—to monitor post-fire soil erosion and ash transport from the hillslopes. All plots were constructed following the methodology of (Robichaud and Brown 2002). Plots were ∼8 m long × 4 m wide and installed in steep terrain (average slope: 40%) where runoff and erosion are likely to occur. Plot length, width and slope gradient were homogeneous within and between fire severities. Sediment trapped by the fences was collected and weighted on 5 dates in the first year after the fire (supplementary table 9). Subsamples were taken and oven-dried at 105 °C for 48 h to calculate moisture and dry mass of the eroded sediments. Sediment yields were calculated as the total mass of dry sediment eroded per unit area of the erosion plots. Mean metal concentration values were measured in eroded material obtained from the sediment fences to characterise metal mobilisation within the hillslope sediments. Metals were quantified following the same procedures as the *in situ* ash and peaty soil samples, with full chemical characteristic determination described in the supplementary material.

2.6. Stream sampling and characterisation of rainstorm events

A monitoring station was established at the catchment outlet (draining ∼1.8 km^2; figures 1(A) and (B)) 13 d after wildfire ignition and before the first rainstorm. Submersible autosampler sensors measured water level (converted to flow via a rating curve), turbidity, EC, and pH at 15 min intervals for 9 months post-wildfire from 12 July 2018 to 17 March 2019. An ISCO 3700 automatic sampler collected hourly particulate (suspended sediments; SS) and solute samples during storms. Solutes were measured in all rainstorm events, while metals in the suspended sediments were analysed in Storms 2, 4, and 5. Stream solutes sampled were analysed with ICP-OES at the Water Sciences Laboratory at the University of Birmingham UK. An extensive description of catchment instrumentation and laboratory methods for solutes are described in Marcotte *et al* (2024). Suspended sediments were analysed ICP-OES at the Department of Geography at University of Manchester UK, following the same ICP-OES protocol described herein for pXRF confirmatory samples.

Precipitation data (15 min intervals) were sourced from a station ∼3 km away (#559586 Greenfield). Five major rainstorm events (figures 1(D) and (E)) were analysed: Storm 1 (13–14 July 2018), Storm 2 (28–30 July 2018), Storm 3 (8–9 September 2018), Storm 4 (6 March 2019), and Storm 5 (16–17 March 2019). Using the storm event data collected with the autosampler, a storm event was defined as a clear rise in the flow with a first $\geqslant$1% increase in discharge within four hours of the discharge peak after the onset of rainfall, and the end of the event was the first time there was $<$1% decrease in discharge. Multipeak events were considered as one storm event in the analyses if the initial discharge peak value did not fall below 50% of the maximum discharge peak on the receding limb before increasing again. Finally, we calculated precipitation intensity and maximum depth of rainfall in any 30 minute period (I30Max) during each rainstorm event to determine how flow dynamics and precipitation patterns may influence metal movement behaviour.

2.7. Lake sediment core collection and chemical composition

To assess metal export towards the receiving reservoir, the sediments from the lakebed surface sediments of Cowbury Dale Reservoir (figure 1(B); Warburton 2023) were sampled with a gravity core obtained after the first two large rainstorm events following the wildfire (figures 1(D) and (E)). The burnt area of Saddleworth Moor drains several sub-catchments most of which contain reservoirs constructed in the late 19th and early 20th centuries. Cowbury Dale Reservoir—built in the 1890s to control water flow for industrial purposes—drains a catchment area of ca. 2 km^2 that includes the central part of the fire-affected moorland (figure 1(A)), with burnt area reaching the water's edge. A sediment core was obtained at the distal end of the long axis of the reservoir, close to the dam wall where the reservoir was deepest. Cores were sampled using a 100 mm diameter gravity corer (Boyle 1995). Extruded cores were subsampled at 2.5 mm contiguous intervals. Sediment geochemistry was determined via energy dispersive x-ray fluorescence using a XEPOS 3 ED-XRF (Spectro-Ametek) for all the samples. Full laboratory procedures are described in the supplementary material.

3. Statistical analyses and calculations

Summary statistics were calculated for ash chemistry, soil chemistry, ash loads, sediment fence loads and particle chemistry, XRF metal concentrations and for metals in dissolved and particulate fraction of the streamflow. We applied the Shapiro Wilk test to ash chemistry, soil chemistry and ash loads to assess data normality, W statistics and p-values (reported in supplementary table 6). If data met normality assumptions (p-value $\geqslant 0.05$), then unpaired t-tests (parametric) were utilised; otherwise, a Mann-Whitney U test (nonparametric) was utilised when normality assumptions were not met. An unpaired t-test was used to compare concentrations of Al, Cu, Ni and Pb in ash from HS areas ($n = 4$) to ES areas ($n = 4$). Similarly, an unpaired t-test was used to compare concentrations of Al, Cu, Ni and Pb in soil samples from HS areas ($n = 4$) to ES ($n = 4$). Mann Whitney U test was used to compare ash loads of HS areas ($n = 30$) to ES ($n = 30$). Significance level is set at $p \leqslant 0.05$. Detailed information about results for each statistical analysis is provided in supplementary tables 2–6.

A principal component analysis (PCA) was applied to the lake core data to evaluate which elements were associated and correlated to each other, and which elements were associated to a certain depth of the core. The first two components (figure 3(B)) together explain 72% of the variance. All statistical analyses were completed in R Statistical software version 4.2.1 (R core team 2022) using the *stats* package. The PCA was performed using the *prcomp* function within the *stats* package, where data were zero-centred and scaled before performing the PCA using the *centre* and *scale* arguments within the *prcomp* function.

We applied a two-source mixing calculation using lead (Pb) and aluminium (Al), which calculated with equation (1):

$$\left(\frac{\mathrm{Pb}}{\mathrm{Al}}\right)_S = f_F\left(\frac{\mathrm{Pb}}{\mathrm{Al}}\right)_F + f_N\left(\frac{\mathrm{Pb}}{\mathrm{Al}}\right)_N \tag{1}$$

where $(\mathrm{Pb/Al})_S$ represents the measured Pb/Al ratio for the entire sediment core; $(\mathrm{Pb/Al})_F$ represents the Pb/Al ratio of flux of wildfire related sediments, assumed to be at the top of the core; and $(\mathrm{Pb/Al})_N$ represents the Pb/Al ratio at the bottom of the lake core unaffected by a large wildfire event and thus the natural signal of sediment delivery to the lake. The fraction of sediment from fire-affected source (i.e. top 0.25 cm of the lake core) is represented as f_F and the fraction of non-wildfire impacted sediment flux is shown as f_N. The average values of the Pb/Al ratio from the bottom 4 cm of the core were used (20 cm–24 cm) as values for $(\mathrm{Pb/Al})_N$, as there were no large wildfire events within the catchment aligning with the calculated ages of this depth range. The mass balance equation (equation (2)) was substituted into the mixing calculation (equation (1)), where the mass balance equation is as follows:

$$f_F + f_N = 1. \tag{2}$$

And the re-written mixing calculation with the mass balance substitution for f_N is shown as equation (3):

$$\left(\frac{\mathrm{Pb}}{\mathrm{Al}}\right)_S = f_F\left(\frac{\mathrm{Pb}}{\mathrm{Al}}\right)_F + (1 - f_F)\left(\frac{\mathrm{Pb}}{\mathrm{Al}}\right)_N. \tag{3}$$

4. Results

Burn severities across the burnt Moor ranged predominately from moderate to extreme, based on the dNBR derived from remote sensing (figure 1(A)). High and extreme burn severity areas (hereafter HS and ES, respectively) accounted for over 75% of the burnt area within the burn perimeter.

Samples of the ash layer and underlying burnt peaty soils were collected for chemical analysis from HS and ES sites, based on the *in situ* burn severity classifications in the field, rather than from the dNBR map. We did not sample unburnt or low burn severity areas because they were limited in extent, and the HS and ES areas were considered to be the most problematic for contaminant export. We found an enrichment of Al, Ni and Pb in ash deposits relative to underlying burnt peaty soils (ER calculated: ash:soil), especially in ES areas (ER 2.2, 2.1 and 1.9, respectively; supplementary table 1), suggesting greater accumulation of these metals in the ash relative to the underlying burnt soil. Conversely, the ER of metals in HS areas were slightly lower comparatively for Al, Cu and Pb (0.7, 1.3 and 1.1, respectively).

Patches of ash and burnt material, which are highly susceptible to mobilisation via water and wind (Bodí *et al* 2014), blanketed the ground at Stalybridge Moor post-wildfire. Ash production on the hillslopes, measured through a series of transects and expressed as ash loads (kg m^{-2}), increased significantly with burn severity (Mann Whitney *U; W* value 857; p-value $\leqslant 0.001$). Extreme burn severity areas, where we observed patches of white and grey ash, led to the highest ash production on average (3.60 ± 0.63 kg m^{-2};

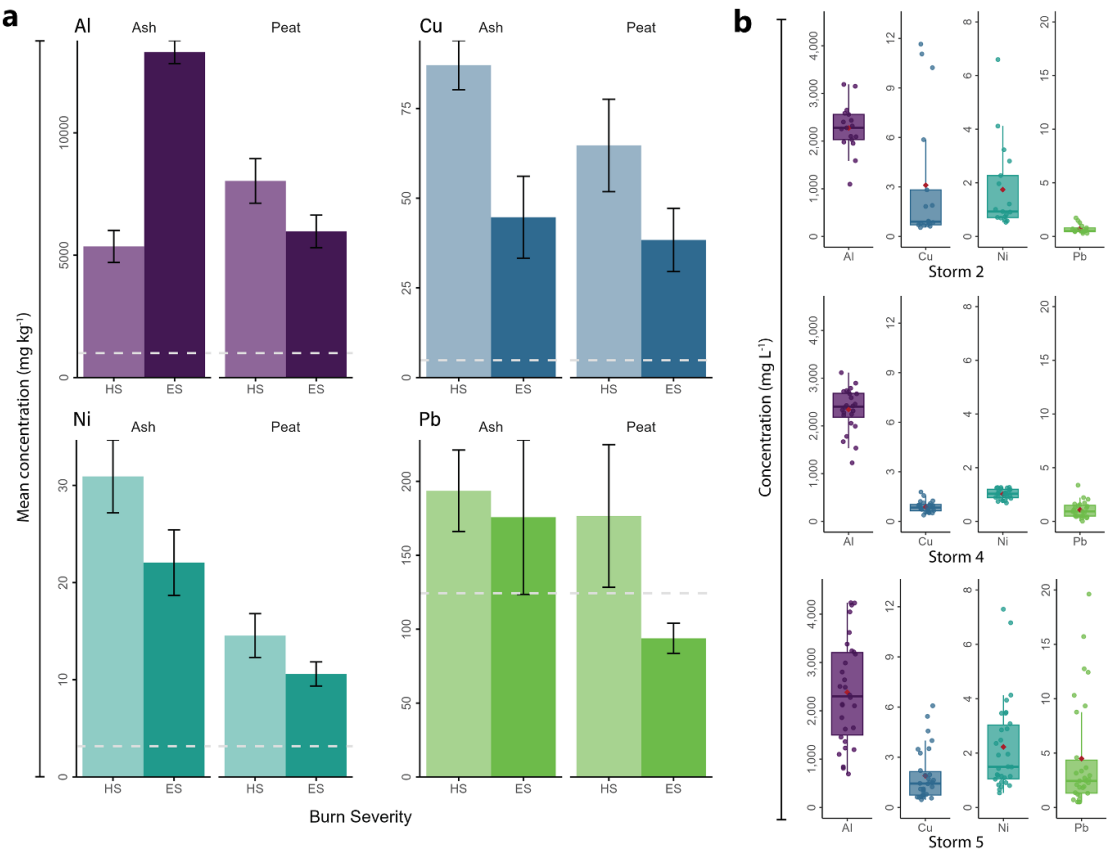

Figure 2. Metal concentrations in particulate form. | (a) Mean metal concentrations measured in ash and peat samples at high burn severity locations (HS) and extreme burn severity locations (ES). Standard error of the mean is denoted with black error bars. The light grey line represents metal concentrations in unburnt peat reported by a study in the region (Tipping *et al* 2003), as a comparison for potential baseline metal values in unburnt areas. (b) Metal concentration in stream suspended sediment (SS) during Storm 2 (summer), Storm 4 (spring) and Storm 5 (spring). The dots on each box plot represent individual data points. The dark coloured line laying horizontally across each box plot denotes the median value and the pink dot denotes the mean.

supplementary table 8), with ash loads ranging from 0.17 kg m^{-2} up to 13.63 kg m^{-2}. Ash production was much lower on average (0.22 $\pm$ 0.02 kg m^{-2}; supplementary table 8) in HS areas and consisted of mostly black ash, with ash loads ranging from 0.04–0.52 kg m^{-2}.

The chemical composition of ash produced in HS areas resulted in higher average concentrations of Cu, Ni and Pb compared to ES areas (figure 2(A); supplementary table 2). In contrast, the average concentration of Al in ash was significantly higher in ES areas (13 301.35 $\pm$ 47.52 mg kg^{-1}; unpaired *t*-test; *p*-value < 0.01). Peaty soils at HS locations had slightly higher metal concentrations on average, compared to the peat in ES areas (figure 2(A); supplementary table 2), though these differences were not statistically significant (unpaired *t*-test; *p*-value > 0.05). In addition, we measured metals along the burnt soil-ash top layer via hillslope pXRF transect and gridded surveys. Values of Pb concentrations along the sampling transect, for example, ranged from 5.52–2330.58 mg kg^{-1} (median 400.79 mg kg^{-1}; supplementary table 7), with higher values of Pb associated with ash-covered locations, rather than char and exposed peat on the ground surface. Cu and Ni values follow a similar spatial pattern (supplementary figures 1(A) and (B)). We observed a wide range of Cu, Ni and Pb values from the pXRF survey, where distinct pockets of metals exist in the landscapes in which stores of metals varied several orders of magnitude, even at small distances of 5 m or less (supplementary figure 1) (Shuttleworth *et al* 2017).

Downslope export of ash and peat material via water erosion captured via sediment trapping fences along the burnt hillslope (figure 1(C)) was highest on average in ES plots (0.10 $\pm$ 0.03 kg m^{-2}; supplementary table 9) compared to HS plots (HS; 0.02 $\pm$ 0.002 mg kg^{-2}; supplementary table 9) measured over one year post-wildfire (17 July 2018–16 July 2019). Metals measured in the sediment from the hillslope fences were quantified (table 1) beginning around the timing of Storm 2, a large multi-peak discharge event (figure 1(E)). In general, metals Al, Cu, Ni and Pb from fences in ES areas peaked around the time of Storm 3 in the autumn (~3 months post fire; table 1). Metals in sediment from fences in HS areas generally followed a similar pattern, except for Cu, where its highest concentration was observed in the first sediment collection date around Storm 2 (84.48 mg kg^{-1}; table 1). In the final two collection dates (December 2018 and July

Table 1. Total concentration of metals measured in sediments collected from erosion sediment fences at a certain sediment collection date, per burn severity (HS or ES). Nd indicates no data were collected—primarily in the timeframe prior to the first rainstorm event in this study (Storm 1).

Sed. collection date	Association with storm event	Burn Sev.	Al (mg kg^{-1})	Cu (mg kg^{-1})	Ni (mg kg^{-1})	Pb (mg k^{-1})
nd	Storm 1	nd nd	nd nd	nd nd	nd nd	nd nd
03/08/2018	Storm 2 on 30 July	ES HS	9201.00 2284.67	59.73 84.48	14.86 14.17	224.66 78.82
18/09/2018	Storm 3 on 9 September	ES HS	9620.36 2859.52	56.17 77.19	15.14 22.59	200.91 96.50
19/09/2018	—	ES HS	12 987.42 3328.75	79.26 49.31	24.71 12.02	344.85 92.40
22/10/2018	—	ES HS	10 874.92 3130.48	66.61 80.39	19.46 16.09	262.41 95.43
06/12/2018	—	ES HS	7839.48 2637.28	55.81 61.57	16.31 14.73	197.85 105.35
16/07/2019	Storm 4 and 5 on 9–14 March	ES HS	5059.21 3677.65	34.68 43.42	12.58 17.14	150.84 100.93

2019, one year post-wildfire), metal concentrations from sediments in the hillslope sediment fences in ES areas declined, but conversely in HS areas Pb concentrations still slightly increased after Storm 3. The latter suggests a potential delayed Pb mobilisation or, alternatively, a prolonged response in HS areas compared to ES areas.

Median concentrations of dissolved Al, Cu, Ni and Pb measured in stream water during the analysed rainstorm events (figures 1(D) and (E)) were initially low following the wildfire in the summer Storms 1 and 2, and only increased ∼3 months later (Al, Ni and Pb; Storm 3 in the autumn). Dissolved concentrations of Al, Ni and Pb were highest in Storm 3, aligning with the peak Al, Ni and Pb concentrations measured in eroded material at sediment fences in ES areas (table 1)—where highest erosion during these events were measured. Dissolved Cu, however, peaked later in the following spring (Storms 4 and 5).

Metal concentrations in the suspended stream sediments (SS) were higher and peaked later than the dissolved fraction. Aluminium (Al) had the highest median concentration (2,279.35 mg l^{-1}) compared with the other metals, which aligns with the high Al concentrations in source and eroded materials (peat soils and ash) (figure 3(B)). The median concentrations of Al, Cu, Ni, and Pb in SS were higher in the spring storm events (Storms 4 and 5; figure 2(B)), compared to Storm 2 in the autumn (figure 3(B)), indicating a potential delay or prolongation in the metal flux in response to wildfire, rather than an acute-only impact. The spring rainstorm events, particularly Storm 5, were characterised by high antecedent moisture during the monitoring period (7 day antecedent rainfall of 82.4 mm), highest precipitation intensity (1.8 mm h^{-1}) and largest discharge of the observed rainstorm events in this study (figure 1(E); supplementary table 10), which likely contributed to greater runoff generation and enhanced transport of metal-bound particulates (Wichman *et al* 2024, Murphy *et al* 2025) compared to the other rainstorm events that were analysed in our study.

In the receiving reservoir sediments, metal concentrations were enriched at the top of the lake core (⩽1.25 cm) obtained from the reservoir (figures 3(A) and (C)), aligning with the timing of the wildfire. Baseline metal concentrations for the reservoir was illustrated by flatter profiles for the deeper sediments (figure 3(C)). The Al peak did not align with the peak of Cu, Ni and Pb, which may potentially be due variation in timing of different fire-related material delivery to the reservoir, as observed at the sediment fences (table 1). Loss on ignition (LOI%) and particle size (D_{50}) decreased at the top of the lake core (figure 3(C)), suggesting that the increase in metals was not controlled by organic matter alone (Pompeani *et al* 2020). For example, peat material likely eroded from the catchment, but the fine metal-rich ash been delivered to the surface waters after the wildfire most likely constituted much of the top of the core. Aluminium concentrations were negatively correlated with LOI% in PC space (figure 3(B)), suggesting that Al is supplied from mineral substrate sources rather than organic sediment sources. Pb and Cu are most associated in PC space with upper portions of the lake core (figure 3(B)) and therefore likely to be sensitive to

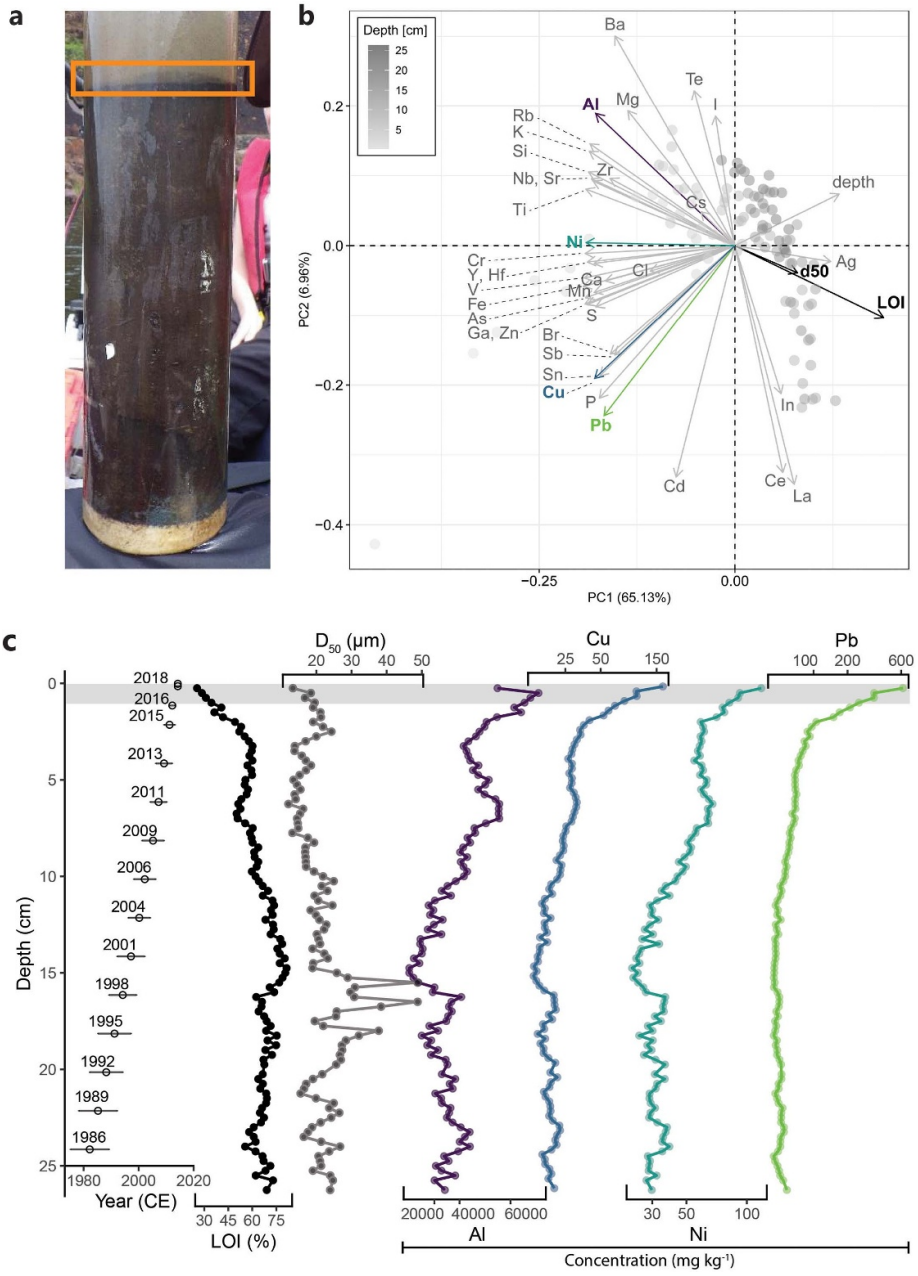

Figure 3. Metal-rich wildfire sediment accumulation in receiving reservoir. | (a) Lake core obtained from Cowbury Dale Reservoir for analysis of metal concentration. The orange box at the top outlines ashes and burnt materials in the top layer. (b) Principal component analysis (PCA) of all measured elements and variables from the lake core. Loss on ignition (LOI), sediment size (D_{50}) and metals Al, Cu, Ni and Pb are bolded and coloured for emphasis and their concentration throughout the length of the core is shown in (c). LOI% is the black line and D_{50} is the dark grey line. All metal concentrations (Al, purple line; Cu, blue line; Ni, teal line; Pb, light green line) are graphed in log concentration (mg kg^{-1}) to better highlight additional peaks in lower portions of the lake core.

disturbances. The study region represents a hotspot for Pb deposition in the UK (Ander *et al* 2012), and Pb and Cu more likely have anthropogenic origins (Shotbolt *et al* 2006).

Given the likelihood of different Al and Pb sources, we applied a two-source mixing model using a Pb:Al ratio to estimate the fraction of Pb-enriched sediment flux to the lake that is due to the wildfire. The flux of Pb released to the reservoir following the wildfire in the top 0.25 cm was ten times (10x) higher than the background rate of Pb flux for the rest of the surface sediment lake core, with an estimated flux of $\sim$31 kg m^{-2} yr^{-1} in the aftermath of the wildfire, assuming an even distribution of burnt materials delivered to the lake across the Cowbury Dale Reservoir (surface area $\sim$12 700 m^2) of wildfire-associated material in the top 0.25 cm of the lakebed sediments. Radiometric dating, combined with visual inspection of sediment and modelling evidence herein, indicate that materials at the top of the lake core—and therefore likely on the surface of the lakebed—are clearly deposits resulting from the wildfire.

5. Discussion

5.1. Metal concentrations in ash and hillslope deposits across different burn severities

We found an enrichment of Al, Ni and Pb in ash deposits relative to underlying burnt peaty soils (ash:soil), notably in ES area. This suggests that wildfire released metals stored in vegetation and peat deposits, and concentrated them in the hillslope ash deposits, where they can be more easily re-distributed within, or exported from, the catchment, thus posing contamination risks for downstream water bodies. Given the likelihood of spatially variable metal concentrations in pre-fire topsoil, it is possible that the calculated ERs may overestimate or wildfire-induced metal enrichment if topsoil metal concentrations were inherently higher than those in the rest of the peat layers. Without pre-wildfire soil metal concentrations, however, we cannot fully disentangle these dynamics.

The actual metal concentrations in ash and peaty soils from HS areas were, in most cases, higher than in ES areas (figure 2(A)), which contrasts with studies showing that metal concentrations in wildfire ash are typically increasing with fire burn severity (Rust *et al* 2019, Paul *et al* 2022). Variability of ash composition can be attributed to both burn severity and pre-wildfire spatial heterogeneity of metal concentrations throughout the landscape in the peaty soil layers. Comparable blanket peat systems in the region show spatially variable metal concentrations in unburnt peat, both vertically in the peat profiles and horizontally in the landscape (Lawlor and Tipping 2003, Rothwell *et al* 2010, Shuttleworth *et al* 2017). Additionally, a study in the Southern Pennines, UK reported concentrations of Al, Cu, Ni and Pb that were below values found in this study (figure 2(A)) (Tipping *et al* 2003).

The study catchment and regional blanket peat systems have a complex erosional history (Evans and Warburton 2007), thus metal concentrations can additionally vary with depth, either due to initial accumulation and storage, or because of ongoing erosion that can expose different soil profiles. Combustion type (i.e. flaming fire or smouldering) and the resulting burn severity introduces additional variability of ash and topsoil metal concentrations, both physically and chemically, also evidenced by the range of ERs from this study. For example, Pb and Cu have been shown to be better retained in peaty soils during lower-temperature burn than compared to a more extreme burn temperature (Li *et al* 2023), highlighting the complexity in metal bioavailability and distribution during and post-fire. A wildfire with a severe and deep burn, such as smouldering combustion, can completely consume large peat layers (Benscoter *et al* 2011, Marcotte *et al* 2022), potentially reaching deeper legacy metal stores (∼10–15 cm) or lithogenic compounds, and reducing them ash. This may expose peaty soils at the surface with higher metal concentrations. In contrast, a surface or shallow burn may only remove the vegetation layer or topsoil and produce a less metal enriched ash, resulting in the large range and spatial variability of metal concentrations across the burnt hillslope. Future studies would benefit from additional knowledge of pre-wildfire metal concentrations, which is currently lacking. Such data can serve as an important potential predictor of metal enrichment and/or release (McCarter *et al* 2024), especially in regions such as our study area where the spatial pattern of metal contamination is influenced by pre-wildfire erosional patterns in the catchment.

5.2. Mobility of ash and burnt materials

Ash loads observed in our study (0.4–136.3 t ha^{-1}) are generally lower than reported in other burnt peatlands (e.g. 41–327 t ha^{-1}) (Marcotte *et al* 2022). These differences could be attributed to variations in factors such as water table position, slope, vegetation composition and peat thickness between study sites. Metal solubility in both ash and peaty soil samples were low (supplementary table 2), often below LOD at the 1:20 dilution factor used in the extraction, indicating very low soluble concentrations if present. This suggests that, while rainfall between the wildfire and sample collection (totalling 23 mm over 6 d–4 d with rainfall) likely contributed to loss of soluble components via leaching (Santín *et al* 2015, Sánchez-García *et al* 2023), the main metal export from the catchment is associated with the transport of ash material.

Despite the highest sediment production rates measured from sediment trapping fences in ES areas, only ∼10% of average sediment from the monitoring period were delivered in ES areas during Storm 2, with increasing amounts measured in the springtime. In HS areas, however, ∼35% of average sediment delivery occurred during Storm 2. Sediment transport gradually decreased towards springtime, likely due to the exhaustion of easily transportable ash on the soil surface in HS areas where its availability is lower than at ES areas. This may be due to the supply of erodible material being more limited at HS plots compared to ES plots. If a large portion of material at the HS plots was transported and released from the catchment during the autumn and timeframe around Storm 2, less material will have remained available for transport during subsequent storm events. In contrast, ES plots still contained larger amounts of ash and metal-rich peat soil. While retention of the metal-rich sediments on the hillslopes most likely limited strong acute impacts on the fluvial system, it enhanced the potential for legacy effects. Consequently, different burn severities across the

landscape will modulate timing and duration of metal-rich sediment movement, thereby affecting peatland potable water resources.

Metal concentrations measured in sediments from the hillslope sediment trapping fences were analysed beginning at Storm 2 of the monitoring period (table 1). Metal concentration in these sediments around the time of Storm 2 were in the same order of magnitude to that of metal concentrations in the ash, especially in HS areas. For example, Pb concentrations in eroded material were 224.66 mg kg^{-1} (ES areas) and 78.82 mg kg^{-1} (HS areas), while Pb concentrations in ash were 175.76 mg kg^{-1} (ES areas) and 193.62 mg kg^{-1} (HS areas). This suggests that post-wildfire, hillslope eroded material was initially largely comprised of ash. In general, metal concentrations in eroded material decrease throughout the post-wildfire monitoring period (table 1), in line with progressive loss of ash from the hillslopes. Some metal loss via transport down slope and/or incorporation into the sub-surface peat soil matrix may have also occurred, however, this was not quantified in our study.

The immediate aftermath of a wildfire is typically characterised by enhanced mobilisation and transport of burnt materials depending on the timing and intensity of post-fire rainfall events (Shakesby and Doerr 2006), where run-off is potentially laden with metals in the months—and sometimes years—following wildfire. Our data indicate that, while post-wildfire transport of metal-rich hillslope material was initially high in some locations (table 1), the peak of sediment and metal transport in the streamflow did not necessarily occur in storm events immediately post-wildfire. This is not unusual, as peak erosion can be delayed until a storm event of sufficient magnitude can facilitate mobilisation and downslope transport of solids (Moody *et al* 2008). This delay in the typical post-fire hydrological and erosion response can occur in conditions with gentle slopes, soils with high infiltration rates and relatively uniform rainfall dynamics, such as at our study site. In blanket peatlands, which form in wet environments, the rapid recovery of vegetation (i.e. mosses, grass, bracken or heather) can reduce overall erosion risks more quickly compared to less humid climates. This underscores the need for continued and frequent monitoring of wildfire-impacted peatland catchments—perhaps even beyond one year post-wildfire—to accurately assess the evolution of environmental impacts and subsequent recovery.

5.3. Metal export to fluvial systems

Metal concentrations were orders of magnitude higher in the SS (figure 2(B)) compared to the solutes during all rainstorm events (supplementary tables 11 and 12), in line with the low availability of water-soluble metals observed in the ash and peaty soil samples (supplementary tables 2 and 3). Overall, though, dissolved concentrations of metals were comparable to other burnt peatland systems (e.g. Canada; Emmerton *et al* 2020). Dissolved metals measured at the stream monitoring location were observed to be below drinking water standards (Water, England and Wales 2016). Moreover, the streamflow from the small headwater catchment streamflow in our study provides a relatively minor contribution to the larger downstream system. Taken together, we therefore infer that observed dissolved metal concentrations in the streamflow after the wildfire event in this study were likely minor and transient enough to not have adversely impacted the greater water supply network during the timeframe of our study.

We observed a delay in the SS metal flux response until the spring rainstorm events. This can be attributed to various factors, including re-suspension and transport of sediment trapped on the hillslopes, varying precipitation amount and intensity being a catalyst for activation of different metal-laden sediment source zones, and—to a lesser extent—dissolved metal source zones (Marcotte *et al* 2024). Substantial in-channel sediment storage of burnt materials was observed in the field, including eroded peat, ash and mineral sediments. This was accumulated and stored in the pools along channel margins and in up-stream riverbed sediments, potentially sourcing sediment internally from the floodplain or local cutbanks into the peat stream channel bank. These materials, along with ashes and peat likely deposited in over-bank flows, may represent a delayed flux of material available to be preferentially re-suspended and transported in subsequent rainstorm events (Ciszewski and Grygar 2016). Such processes would also explain the continued delivery of metal-rich SS in the stream flow during the spring (figure 2(B)), even when metals measured at ES erosion plots peaked in autumn (table 1). These factors, due to slope or in combination with each other, could contribute to a chronic and potentially substantial transfer of metal-rich material after wildfire occurrence, even if source zones were not limited to the hillslopes.

In summary, the observed patterns of metal-rich hillslope transport into the autumn (table 1) and the increase in median metal concentration in stream particulates in the springtime post-wildfire (figure 2(B)) indicate that continued accumulation of metal-rich sediments on the lakebed may occur for at least nine months (figure 4). Magnitudes of metal pulses will likely fluctuate with erosion events or future disturbances, as observed in the lake core below ∼10 cm (figure 3(C)). Together, the potential for prolonged legacy metal release, transport and accumulation extends beyond the immediate post-wildfire period, pointing to the

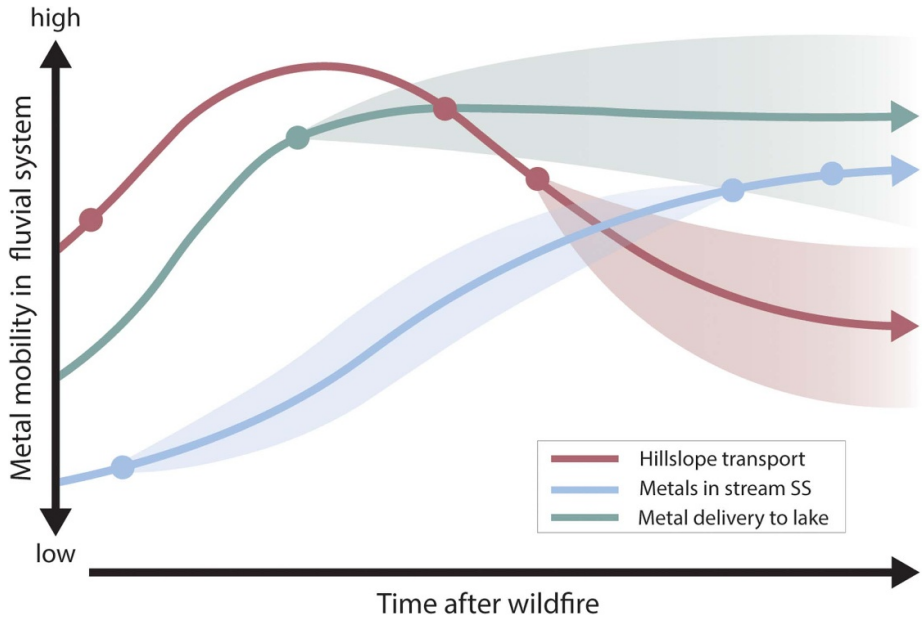

Figure 4. Visual conceptualisation of metal-rich material transport within the catchment following the wildfire event. | We highlight observed (circles on lines) and inferred or likely (lighter coloured shading around the line) timing of metal particulate transport from hillslopes into the receiving reservoir, guided by findings and observations from this study. Metal concentrations in the hillslope burnt ash peat deposits was high compared to unburnt background values reported. Mobility of metal-rich particles, measured at sediment fences, peaked in the autumn ∼3 months post-wildfire. Given drought conditions at the time of wildfire, initially metal-rich sediment transport within the streams is limited and showed an increase in the spring season (∼9 months post-wildfire). The lake core was obtained shortly following the wildfire and already showed high metal concentrations in the top layer. Given the continued delivery of metal-rich particles observed from sediment fence data and suspended stream data, we postulate that it is likely for high metal accumulation on the lakebed to be sustained several months following the wildfire, which can have implications for legacy metal impacts.

likelihood of complex multi-seasonal patterns of post-fire contaminant dynamics within burnt peat-dominated catchments.

6. Conclusion

In this study, we quantified potentially toxic metals release and transport following the Stalybridge Moor wildfire from source to sink. Specifically, we measured metal concentrations in ash and peaty soil deposits under different burn severities and tracked the transport of metal-bound particulate deposits during rainstorm events to the receiving reservoir. Metal concentrations of hillslope ash and peaty soil samples were spatially variable, but were generally higher than reported baseline values from regional studies with legacy pollutants from industrialised surroundings. Metal concentrations measured in eroded sediments from hillslope sediment fences were highest in the summer and autumn (∼3 months post-wildfire) and generally declined moving to the winter and springtime (∼9 months post-fire), with metal concentrations higher in the extreme burn severity areas compared to lower burn severity areas. In the stream suspended sediment, metals were highest in the observed spring storm events rather than immediately post-fire. Burning released legacy deposits of surficial Pb and other metals from the catchment to the rest of the system, as observed from the high concentrations of metals on the lakebed surface. Whether or not this is sufficient to present a water quality problem at this reservoir either at present day or chronically in future would require further investigation of metal solubility and mobilisation within the lake water column, and deposition rates in the sediments.

Wildfires in temperate peatlands can trigger sudden releases of legacy metals. Depletion of large stores of potentially toxic metals during wildfire events, coupled with leaching losses and existing on-going erosion in blanket peat systems, could outpace future metal deposition leading to declines of in-peat legacy metal stores. As climate-change induced hydrological extremes increase in frequency, magnitude and duration, our findings underscore the urgent need for prolonged monitoring of post-wildfire sediment transport and resuspension dynamics of metal-rich particulates in temperate peatland systems with legacy contaminants.

Data availability statement

Lake core elemental concentrations are publicly available from the UK CEH Environmental Information Data Centre via https://doi.org/10.5285/4f447446-5461-48b2-b154-ff7094176502. Precipitation data used in this study are publicly available the UK Environment Agency Rainfall API (https://environment.data.gov.uk/flood-monitoring/archive). Sentinel-2 satellite imagery used to calculate dNBR in this study are publicly available for download and were obtained from USGS Earth Explorer (https://earthexplorer.usgs.gov/). Historical wildfire log shapefile was obtained via a data request to Moors for the Future Partnership (www.moorsforthefuture.org.uk/about-us/contact-us).

The data that support the findings of this study are openly available at the following URL/DOI: https://doi.org/10.5281/zenodo.15193608. Data will be available from 02 June 2025.

Acknowledgments

Authors are grateful to Ben C Howard, Alexander G Hurley, Danny Croghan, Angeliki Kourmouli, Samantha Leader and Tanu Singh for assistance with data collection in the field and laboratory analyses. S H D, J N and C S were supported by UKRI Natural Environment Research Council (NERC) Grant NE/R011125/1. R C C, E L S and J W were supported by UKRI NERC Grant NE/S011560/1.

Author contributions

C M B, R C C, G D C, S H D, K K, S K, J N, C S, E L S, S U, J W and N K conceived the idea for the study and led data collection. A L M conducted formal data analysis and interpretation. J L, G D C, S H D, J N, J P N, D P P, C S, E L S, J W and N K advised on data analysis and interpretation. J.L. and N.K. were responsible for supervision. A L M, J L and R Í M were responsible for data visualisation. A L M led writing of the manuscript. All authors provided feedback on the manuscript and gave approval for the final manuscript.

Conflict of interest

The authors declare that they have no known competing interests that influence the work reported in this paper.

Ethics statement

This research does not include any use of human or animal subjects, data or tissue.

ORCID iDs

Abbey L Marcotte https://orcid.org/0000-0003-4149-3473
Juul Limpens https://orcid.org/0000-0001-5779-0304
Claire M Belcher https://orcid.org/0000-0003-3496-8290
Richard C Chiverrell https://orcid.org/0000-0002-7307-2756
Gareth D Clay https://orcid.org/0000-0002-8477-2774
Stefan H Doerr https://orcid.org/0000-0002-8700-9002
Stefan Krause https://orcid.org/0000-0003-2521-2248
Kieran Khamis https://orcid.org/0000-0002-5203-3221
Rúna Í Magnússon https://orcid.org/0000-0003-2254-2612
Jonay Neris https://orcid.org/0000-0002-8754-9236
João Pedro Nunes https://orcid.org/0000-0002-0164-249X
David P Pompeani https://orcid.org/0000-0002-3571-4586
Cristina Santín https://orcid.org/0000-0001-9901-2658
Emma L Shuttleworth https://orcid.org/0000-0003-0661-1366
Sami Ullah https://orcid.org/0000-0002-9153-8847
Jeff Warburton https://orcid.org/0000-0003-3589-9039
Nicholas Kettridge https://orcid.org/0000-0003-3995-0305

References

Agbeshie A A, Abugre S, Atta-Darkwa T and Awuah R 2022 A review of the effects of forest fire on soil properties *J. For. Res.* **33** 1419–41

Ander E, Cave M, Johnson C and Palumbo-Roe B 2012 Normal background concentrations of contaminants in the soils of England Available data and data exploration (https://doi.org/10.1016/j.jpainsymman.2011.10.026)
Benscoter B W, Thompson D K, Waddington J M, Flannigan M D, Wotton B M, De Groot W J and Turetsky M R 2011 Interactive effects of vegetation, soil moisture and bulk density on depth of burning of thick organic soils *Int. J. Wildland Fire* **20** 418–29
BGS Geology Viewer 2024 BGS geology viewer *The Geological Map Viewer of Britain* (available at: https://geologyviewer.bgs.ac.uk/)
Bodí M B, Martin D A, Balfour V N, Santín C, Doerr S H, Pereira P, Cerdà A and Mataix-Solera J 2014 Wildland fire ash: production, composition and eco-hydro-geomorphic effects *Earth Sci. Rev.* **130** 103–27
Bowman D M J S, Kolden C A, Abatzoglou J T, Johnston F H, van der Werf G R and Flannigan M 2020 Vegetation fires in the Anthropocene *Nat. Rev. Earth Environ.* **1** 500–15
Boyle J F 1995 A simple closure mechanism for a compact, large-diameter, gravity corer *J. Paleolimnol.* **13** 85–87
Brown L E, Holden J, Palmer S M, Johnston K, Ramchunder S J and Grayson R 2015 Effects of fire on the hydrology, biogeochemistry, and ecology of peatland river systems *Freshw. Sci.* **34** 1406–25
Brown P A, Gill S A and Allen S J 2000 Metal removal from wastewater using peat *Water Res.* **34** 3907–16
Buurman P 1996 *Manual for Soil and Water Analysis* (Backhuys Publ.)
Chafer C J, Santín C and Doerr S H 2016 Modelling and quantifying the spatial distribution of post-wildfire ash loads *Int. J. Wildland Fire* **25** 249–55
Ciszewski D and Grygar T M 2016 A review of flood-related storage and remobilization of heavy metal pollutants in river systems *Water Air Soil Pollut.* **227** 239
Emmerton C A *et al* 2020 Severe western Canadian wildfire affects water quality even at large basin scales *Water Res.* **183** 116071
Evans M and Warburton J 2007 Geomorphology of Upland Peat
Forestry Commission 2023 Wildfire statistics for England: Report to 2020-21
Garcés-Pastor S, Fletcher W J and Ryan P A 2023 Ecological impacts of the industrial revolution in a lowland raised peat bog near Manchester, NW England *Ecol. Evol.* **13** e9807
Graham A M *et al* 2020 Impact of the June 2018 Saddleworth Moor wildfires on air quality in northern England *Environ. Res. Commun.* **2** 031001
Hageman P L 2007 U.S. geological survey field leach test for assessing water reactivity and leaching potential of mine wastes, soils, and other geologic and environmental materials *Techniques and Methods* (available at: https://pubs.usgs.gov/publication/tm5D3)
Holden J 2006 Chapter 14 Peatland hydrology *Developments in Earth Surface Processes* vol 9 (Elsevier) pp 319–46 (https://linkinghub.elsevier.com/retrieve/pii/S0928202506090146)
Ipcc 2022 *Global Warming of 1.5 °C: IPCC Special Report on Impacts of Global Warming of 1.5 °C above Pre-industrial Levels in Context of Strengthening Response to Climate Change, Sustainable Development, and Efforts to Eradicate Poverty* (Cambridge University Press) (www.cambridge.org/core/product/identifier/9781009157940/type/book)
Jones M W *et al* 2022 Global and regional trends and drivers of fire under climate change *Rev. Geophys.* **60** e2020RG000726
Joosten H and Clarke D 2002 *Wise Use of Mires and Peatlands: Background and Principles Including a Framework for Decision-making* (International Peat Society ; International Mire Conservation Group)
Keeley J E 2009 Fire intensity, fire severity and burn severity: a brief review and suggested usage *Int. J. Wildland Fire* **18** 116
Kettridge N, Turetsky M R, Sherwood J H, Thompson D K, Miller C A, Benscoter B W, Flannigan M D, Wotton B M and Waddington J M 2015 Moderate drop in water table increases peatland vulnerability to post-fire regime shift *Sci. Rep.* **5** 8063
Lawlor A J and Tipping E 2003 Metals in bulk deposition and surface waters at two upland locations in northern England *Environ. Pollut.* **121** 153–67
Li X, Wang G, Li Y, Han D, Cong J and Gao C 2023 Aerobic and anaerobic burning alter trace metal availability in peat soils: evidence from laboratory experiments *Eur. J. Soil Sci.* **74** e13385
Liu H, Zak D, Zableckis N, Cossmer A, Langhammer N, Meermann B and Lennartz B 2023 Water pollution risks by smoldering fires in degraded peatlands *Sci. Total Environ.* **871** 161979
Marcotte A L *et al* 2024 Enhanced hydrologic connectivity and solute dynamics following wildfire and drought in a contaminated temperate peatland catchment *Water Resour. Res.* **60** e2023WR036412
Marcotte A L, Limpens J, Stoof C R and Stoorvogel J J 2022 Can ash from smoldering fires increase peatland soil pH? *Int. J. Wildland Fire* **31** 607–20
McCarter C P R, Clay G D, Wilkinson S L, Page S, Shuttleworth E L, Davidson S J, Taufik M, Sigmund G and Waddington J M 2023 Peat fires and the unknown risk of legacy metal and metalloid pollution *Environ. Res. Lett.* **18** 071003
McCarter C P R *et al* 2024 Peat fires and legacy toxic metal release: an integrative biogeochemical and ecohydrological conceptual framework *Earth Sci. Rev.* **256** 104867
Moody J A, Martin D A, Haire S L and Kinner D A 2008 Linking runoff response to burn severity after a wildfire *Hydrol. Process.* **22** 2063–74
Murphy S F, Blake J M, Ebel B A and Martin D A 2025 Intersection of wildfire and legacy mining poses risks to water quality *Environ. Sci. Technol.* **59** 35–44
Nunes J P, Doerr S H, Sheridan G, Neris J, Santín C, Emelko M B, Silins U, Robichaud P R, Elliot W J and Keizer J 2018 Assessing water contamination risk from vegetation fires: challenges, opportunities and a framework for progress *Hydrol. Process.* **32** 687–94
Paul M J, LeDuc S D, Lassiter M G, Moorhead L C, Noyes P D and Leibowitz S G 2022 Wildfire induces changes in receiving waters: a review with considerations for water quality management *Water Resour. Res.* **58** e2021WR030699
Pompeani D P, McLauchlan K K, Chileen B V, Calder W J, Shuman B N and Higuera P E 2020 The biogeochemical consequences of late Holocene wildfires in three subalpine lakes from northern Colorado *Quat. Sci. Rev.* **236** 106293
Price J S, McCarter C P R and Quinton W L 2023 Groundwater in peat and peatlands (The Groundwater Project) (available at: http://gw-project.org/books/groundwater-in-peat-and-peatlands/)
R core team 2022 R statistical software
Renberg I, Persson M W and Emteryd O 1994 Pre-industrial atmospheric lead contamination detected in Swedish lake sediments *Nature* **368** 323–6
Robichaud P R and Brown R E 2002 Silt fences: an economical technique for measuring hillslope soil erosion *Gen. Tech. Rep. RMRS-GTR-94. Fort Collins, CO: U.S. Department of Agriculture, Forest Service, Rocky Mountain Research Station. 24 p.* 94 (available at: https://research.fs.usda.gov/treesearch/4543)
Robinne F-N *et al* 2021 Scientists' warning on extreme wildfire risks to water supply *Hydrol. Process.* **35** e14086
Rothwell J J, Evans M G and Allott T E H 2007 Lead contamination of fluvial sediments in an eroding blanket peat catchment *Appl. Geochem.* **22** 446–59

Rothwell J J, Taylor K G, Chenery S R N, Cundy A B, Evans M G and Allott T E H 2010 Storage and behavior of As, Sb, Pb, and Cu in ombrotrophic peat bogs under contrasting water table conditions *Environ. Sci. Technol.* **44** 8497–502
Rust A J, Saxe S, McCray J, Rhoades C C and Hogue T S 2019 Evaluating the factors responsible for post-fire water quality response in forests of the western USA *Int. J. Wildland Fire* **28** 769
Ryan K C and Noste N V 1985 *Evaluating Prescribed Fires* (USDA Forest Service Intermountain Forest and Range Experiement Station)
Sánchez-García C *et al* 2023 Chemical characteristics of wildfire ash across the globe and their environmental and socio-economic implications *Environ. Int.* **178** 108065
Santín C, Doerr S H, Otero X L and Chafer C J 2015 Quantity, composition and water contamination potential of ash produced under different wildfire severities *Environ. Res.* **142** 297–308
Shakesby R and Doerr S 2006 Wildfire as a hydrological and geomorphological agent *Earth Sci. Rev.* **74** 269–307
Shotbolt L, Hutchinson S M and Thomas A D 2006 Sediment stratigraphy and heavy metal fluxes to reservoirs in the Southern Pennine uplands, UK *J. Paleolimnol.* **35** 305–22
Shuttleworth E L, Clay G D, Evans M G, Hutchinson S M and Rothwell J J 2017 Contaminated sediment dynamics in peatland headwater catchments *J. Soils Sediments* **17** 2637–47
Shuttleworth E L, Evans M G, Hutchinson S M and Rothwell J J 2014 Assessment of lead contamination in peatlands using field portable XRF *Water Air Soil Pollut.* **225** 1844
Shuttleworth E L, Evans M G, Pilkington M, Spencer T, Walker J, Milledge D and Allott T E H 2019 Restoration of blanket peat moorland delays stormflow from hillslopes and reduces peak discharge *J. Hydrol. X* **2** 100006
Sutton O F, McCarter C P R and Waddington J M 2024 Globally-significant arsenic release by wildfires in a mining-impacted boreal landscape *Environ. Res. Lett.* **19** 064024
Tipping E, Smith E J, Lawlor A J, Hughes S and Stevens P A 2003 Predicting the release of metals from ombrotrophic peat due to drought-induced acidification *Environ. Pollut.* **123** 239–53
Warburton J 2023 Sediment short cores from Higher Swineshaw and Cowbury Dale reservoirs, UK, 2018 (available at: https://catalogue.ceh.ac.uk/id/4f447446-5461-48b2-b154-ff7094176502)
Water, England and Wales 2016 The water supply (water quality) regulations 2016 England and Wales *Water Supply* No. 614 (available at: www.legislation.gov.uk/uksi/2016/614/contents)
Wichman G, Johnston S G and Maher D T 2024 Antimony flux and transport dynamics in a mining-impacted river is linked to catchment hydrodynamics and climate oscillations *Hydrol. Process.* **38** e15323
Wu Y, Xu X, McCarter C P R, Zhang N, Ganzoury M A, Waddington J M and de Lannoy C-F 2022 Assessing leached TOC, nutrients and phenols from peatland soils after lab-simulated wildfires: implications to source water protection *Sci. Total Environ.* **822** 153579
Xu J, Morris P J, Liu J and Holden J 2018a Hotspots of peatland-derived potable water use identified by global analysis *Nat. Sustain.* **1** 246–53
Xu J, Morris P J, Liu J and Holden J 2018b PEATMAP: refining estimates of global peatland distribution based on a meta-analysis *CATENA* **160** 134–40